COMPARATIVE FEATURES OF BINP AMS AND MICADAS FACILITIES WORKING AT AMS GOLDEN VALLEY, RUSSIA

A V Petrozhitskiy[1,2,3]* • E V Parkhomchuk[1,3,4] • M M Ignatov[1,3] • D V Kuleshov[1,3] • L A Kutnyakova[3] • E S Konstantinov[2] • V V Parkhomchuk[1,2]

[1]Novosibirsk State University, AMS Golden Valley, 2 Pirogova str., Novosibirsk, 630090, Russia
[2]Budker Institute of Nuclear Physics Siberian Branch Russian Academy of Sciences (BINP SB RAS), 11 Acad. Lavrentiev Ave., Novosibirsk, 630090, Russia
[3]Institute of Archaeology and Ethnography (IAET SB RAS), 17 Acad. Lavrentiev Ave., Novosibirsk, 630090, Russia
[4]Boreskov Institute of Catalysis (BIC SB RAS), 5 Acad. Lavrentiev Ave., Novosibirsk, 630090, Russia

ABSTRACT. The AMS Golden Valley radiocarbon analysis laboratory is equipped with two accelerator mass spectrometers: AMS facility from Budker Institute of Nuclear Physics (BINP AMS) and MIni CArbon DAting System (MICADAS-28) from Ionplus AG and two graphitization systems: Automated Graphitization Equipment (AGE-3) from Ionplus AG and Absorption-catalytic setup developed in Boreskov Institute of Catalysis (ACS BIC). The laboratory provides routine ^{14}C analyses of various samples: collagen, cellulose, humic acids, carbonates from sediments, etc. The main focus of the laboratory is to determine the age of archaeological artifacts by radiocarbon dating. This work presents a comprehensive description of the BINP AMS facility, with its operation compared with that of MICADAS in the same laboratory. In 2022, the AMS Golden Valley laboratory participated for the first time in the Glasgow International Radiocarbon Inter-comparison (GIRI). The samples were graphitized on the AGE-3 and subsequently measured in both AMS facilities. A comparison of the results of the two series of experiments, namely AGE-3 + MICADAS-28 and AGE-3 + BINP AMS, is given.

KEYWORDS: AMS facilities, intercomparison, radiocarbon AMS dating.

INTRODUCTION

BINP AMS facility started routine operation in 2011. Until 2019, BINP AMS remained the only AMS in Russia. At that time, the throughput capacity of BINP AMS was about 1000 samples per year and was not sufficient to meet the needs of numerous national scientific institutes. Therefore, in December 2019, a new AMS facility MICADAS (Synal et al. 2007) with AGE-3 graphitization system (Wacker et al. 2010) was installed at Novosibirsk State University. A joint radiocarbon AMS laboratory was established in May 2020 by agreement between four scientific organizations of the Novosibirsk Scientific Center: Novosibirsk State University (NSU), Budker Institute of Nuclear Physics Siberian Branch Russian Academy of Sciences (BINP SB RAS), Boreskov Institute of Catalysis (BIC SB RAS), Institute of Archaeology and Ethnography (IAET SB RAS). The laboratory is registered in Radiocarbon as the AMS Golden Valley radiocarbon laboratory (short index GV). This name was chosen according to the location of the laboratory in Akademgorodok, Novosibirsk, Russia. The Golden Valley laboratory is currently equipped with two AMS facilities, MICADAS-28 and BINP AMS, and two graphitization systems, AGE-3 and Absorption-catalytic setup developed in Boreskov Institute of Catalysis (ACS BIC) (Lysikov et al. 2018). The laboratory performs routine ^{14}C analyses of various samples: collagen, cellulose, humic acids, carbonates from sediments, etc. The main focus of the laboratory is to determine the age of archaeological artifacts by radiocarbon dating.

MICADAS-28 Operation in the AMS Golden Valley Laboratory

The MICADAS accelerator mass spectrometer was specifically designed and intended for routine radiocarbon analysis. The reader is referred to (Synal et al. 2007) for a detailed

---

*Corresponding author. Email: petrozhav@gmail.com

description of the MICADAS design. MICADAS-28 with a fixed permanent magnet ("green" one) was commissioned at the AMS Golden Valley laboratory in December 2019. Between 2020 and 2021, several serious MICADAS-28 incidents occurred due to different factors, including pandemics, sudden changes in indoor temperature and humidity, and insufficient quality of electric power supply. For the safe routine operation of MICADAS and AGE-3, a stable power supply system was designed and installed using a double conversion type (online) UPS unit and a backup diesel generator. Routine sample measurements started in February 2022. By the end of 2022, approximately 1000 samples were measured on MICADAS-28.

BINP AMS Features

BINP AMS incorporating the original design was commissioned in 2011 and by the end of 2022, about 5000 cathodes were measured (Parkhomchuk et al. 2016; Molodin et al. 2019; Nazarov et al. 2022; Shnaider et al. 2023). BINP AMS has several features distinguishing it from other similar facilities (Klyuev et al. 2009; Parkhomchuk and Rastigeev 2009, 2011). The BINP AMS layout is shown in Figure 1. The comparison of the main parameters of MICADAS and BINP AMS is given in Table 1. The main features of BINP AMS are the following: 180º electrostatic bend in the middle of tandem accelerator, vertical installation of the accelerating tubes, and Mg vapor stripping canal (Klyuev et al. 2009).

The carbon ion beam in BINP AMS is produced in the classical design of the sputtering negative ion source with solid cathodes (Figure 2): 1 mm graphite sample cathodes are installed in the sample wheel (1) with 24 mounting positions. The first mounting position is for the mechanical alignment of the sample wheel, and the other 23 positions are for the cathodes. The sample wheel rotation for serial cathode change is performed by a stepper motor through a dielectric shaft (14). The heat of the sample wheel during the ion source operation is removed to the atmosphere through the copper shaft with a sliding vacuum rotation feedthrough (12) and blown away by a heat dissipation radiator (13). The cathode potential is about –25 kV relative to the ground. The body of the ion source is at the cathode potential. The ion source is equipped with a spherical ionizer (3) made of 0.5 mm thick tantalum sheet. The ionizer is heated by a filament with 17A current. The accelerating voltage of Cs ions is maintained at a constant 8 kV, even during sample changes. An insignificant sputtering of the metal gaps occurs between the cathodes, leading to slow wear of the sample wheel cover. This requires the cover to be replaced no more than once a year. The ionizer potential is –17 kV relative to the ground. The C⁻ beam is accelerated after the ionizer by an extractor electrode (4). An electrostatic lens (5) is used to focus the beam.

A negative feature of this ion source is the absence of a gate valve or vacuum lock for the sample wheel change without breaking the vacuum inside the ion source. This feature makes the ion source operation extremely difficult. In particular, when installing a sample wheel with fresh samples, it is necessary also to install a new batch of Cs glass ampoules. We usually install 6 ampoules of 15 mg each. This is followed by a 10–12 hours vacuum pumping and degassing period of the ion source. During the degassing process, the ionizer heating current is gradually increased to the nominal value and ion source HV potentials are applied. Only then can the Cs glass ampoules be crushed. Typical ^{12}C LE currents are 10–15 μA C⁻ during the measurement.

After the ion source, the C⁻ beam enters the low-energy magnetic spectrometer (LE magnet), a 90° electromagnet with 500 mm turning radius and a magnetic field decay factor of 0.5. Unfortunately, the vacuum chamber of the LE magnet is not electrically isolated from the
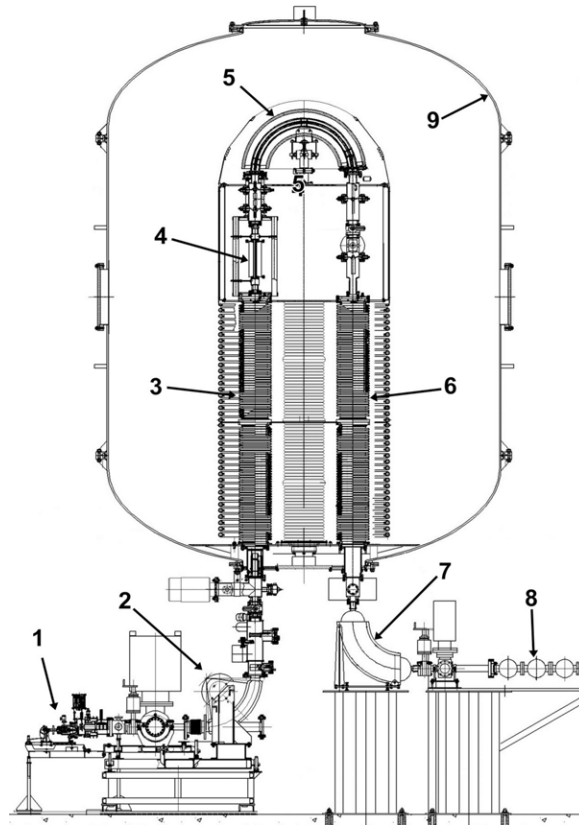
Figure 1   BINP AMS layout: 1—negative ion source; 2—low energy magnetic spectrometer; 3—first accelerating tube; 4—Mg vapor stripping canal; 5—electrostatic 180º bend; 6—second accelerating tube; 7—high energy magnetic spectrometer; 8—time-of-flight ion detector; 9—insulating tank of the accelerator.

ground potential. Thus, the sequential injection of ^{14}C and ^{13}C beams into the accelerator is performed by switching the cathode potential in the ion source: –22.8 kV and –24.5 kV for ^{14}C and ^{13}C, respectively. Changing the beam energy subsequently leads to the need for high-voltage switching of the following five optical elements: ion source electrostatic lens, LE magnet Y stirrer, electrostatic lens at the input of the first accelerating tube, 180° electrostatic bend, and Y stirrer at the input of the second accelerating tube.

After the LE magnet, the beam goes through the first accelerating tube to a terminal voltage of +1 MV. Accelerating tubes are relatively long, with a length of 2 m. The acceleration rate is only 0.5 MeV/m. The ^{12}C beam current is not injected into the accelerating tube, and the remaining currents ^{13}C and ^{14}C are too small to cause vacuum sparks, indicating no need to suppress secondary electrons. As a result, BINP AMS tandem accelerator has no problems with electric strength on the vacuum side. The accelerator voltage is provided by the cascade HV multiplier with serial capacitive coupling, which is limited to +1 MV due to the design features.

Table 1   Comparison of basic MICADAS and BINP AMS parameters.

| Parameter	MICADAS	BINP AMS
Measured isotope	^{14}C only	Now ^{14}C. In the future ^{10}Be, ^{26}Al, ^{129}I
Accelerating voltage	0.2 MV	1 MV
Electrical insulation of HV terminal	Vacuum (10^{-8} mbar)	N_2 1.6 bar(abs)+SF_6 0.05 bar
Accelerating HV source	External commercial high voltage power supply. Compound filled	Cascade HV multiplier with serial capacitive coupling in the accelerator tank
Selected charge state after stripper canal	1+	3+
Stripper material	Gas He	Vapor Mg
^{13}CH, ^{12}CH$_2$ molecule destruction method	Multiple collisions in a thick He target	Coulomb instability in the charge state +3
Total beam transmission	Approximately 46%	Approximately 20%
Magnetic spectrometers	Permanent magnets	Electromagnets (water cooled)
Cs sputtering negative ion source cathodes	Solid + gas cathodes	Solid cathodes only
Number of cathodes in the load. Cathode change method	40 cathodes in magazine. Vacuum lock chamber	23 cathodes in wheel. Partial disassembly of the ion source
Typical ^{12}C LE ion current during measurements	50–70 uA	10–15 uA
Typical ^{14}C statistics on modern samples	Around 600,000 counts ^{14}C (0.13% stat. accuracy)	Around 20,000 counts ^{14}C (0.7% stat. accuracy)
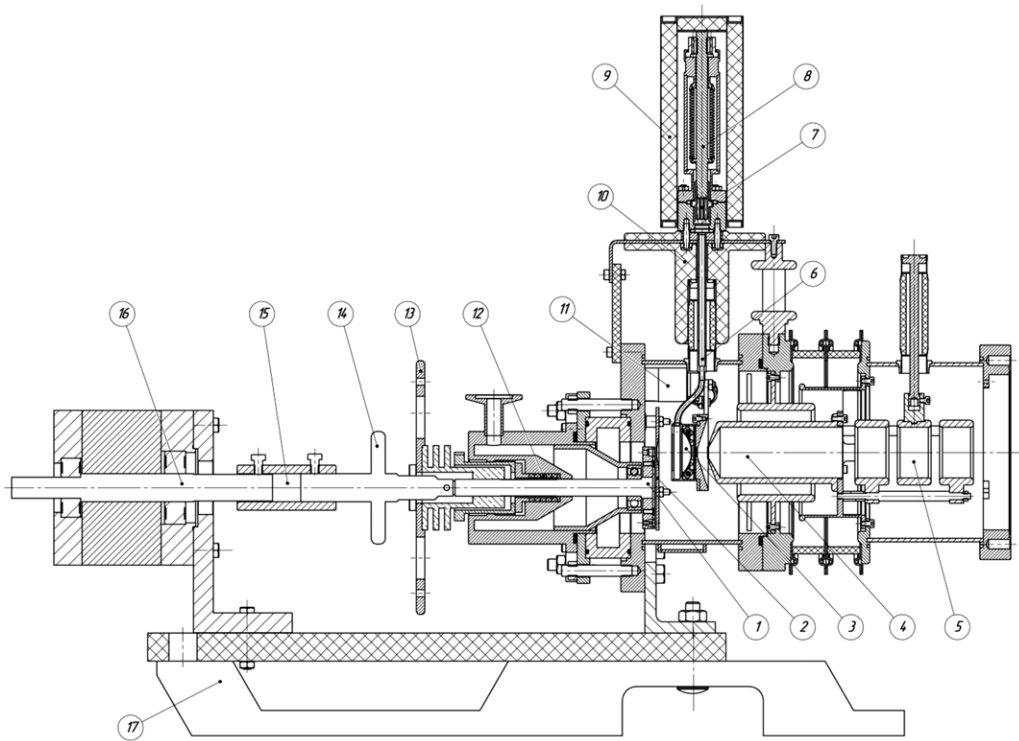
Figure 2   BINP AMS ion source layout (section): 1—sample wheel; 2—diaphragm; 3—ionizer; 4—extractor electrode; 5—electrostatic lens; 6—Cs vapor feedline; 7—Cs ampoule container; 8—ampoule cracker; 9—Cs heater and heat insulation; 10—Cs vapor feedline heater and heat insulation; 11—ionizer mounting shielded ceramic rod; 12—copper shaft with sliding vacuum rotation feedthrough; 13—heat dissipation radiator; 14—dielectric shaft; 15—stepper motor coupling; 16—stepper motor; 17—dielectric base.

After acceleration, the beam enters the charge exchange canal. The BINP AMS uses a magnesium vapor canal (Kluev et al. 2009). Other AMS facilities typically use a gas canal with recirculation. The use of magnesium has several advantages: Mg vapor condenses on cold surfaces and does not worsen the vacuum in the accelerator. This allowed us to get rid of the gas recirculation system and simplify the design of the HV terminal. Improving the vacuum in the accelerating tubes reduces ^{14}C background. The nominal stripper operating temperature is 540–590°C. The stripping efficiency of carbon ions to charge state +3 together with optical transmission gives a total transmission of approximately 20%. The stripper canal is a stainless steel tube with 6 mm inner diameter and 300 mm length. The Mg reservoir is coaxial to the canal. Mg vapor flows out from the reservoir in the middle of the canal through 4 holes with 1 mm diameter. A copper temperature equalizer is put over the Mg reservoir so that the temperature at the edges and in the center of the target is the same. Heating is accomplished by a filament in ceramic insulation. The temperature control is provided by three thermocouples. Vacuum heat shields are used to keep the heat. The nominal power consumption to maintain the Mg temperature is about 50 W. The Mg load is a 200 g cylinder with an outer diameter of 23 mm, wall thickness of 5 mm, and length of 300 mm. These parameters are sufficient for about 2 years of BINP AMS operation. Diaphragms are installed at the inlet and outlet of the target to reduce Mg flow into the accelerator. No electrical strength decrease was observed inside the first accelerating tube during the entire period of the BINP AMS operation.

Immediately after the charge exchange, the beam is filtered with 180° electrostatic bend. The +3 charge state is selected. The dissociated $^{12}CH_2^{3+}$ and $^{13}CH^{3+}$ molecular fragments are completely eliminated before the second accelerating tube due to the incorrect energy-to-charge ratio (Parkhomchuk and Rastigeev 2009).

After the electrostatic bend of 180°, the beam is accelerated to the ground potential in the second accelerator up to the energy of 4.025 MeV. Both accelerating tubes have a vertical installation. Together with a high-voltage cascade generator, they form an accelerating column. Located at the top of the column is a high-voltage terminal with a charge-exchange canal, 180° electrostatic bend, of and four pairs X-Y stirrers. The BINP AMS tandem accelerator is put inside the insulating tank with an outer diameter of 3.2 m, a height of 4.6 m, and a volume of 31.2 m^3. The electrical insulation of the HV terminal is provided by a mixture of 1.6 bar (abs) nitrogen and 0.05 bar sulfur hexafluoride (SF_6).

After the tandem accelerator, the beam is finally filtered in a high-energy magnetic spectrometer, and the ^{13}C current is measured by an off-axis Faraday cup to normalize the ^{14}C count. BINP AMS uses a time-of-flight (TOF) type final detector. It has two flight intervals of 0.3 m and a 0.5 ns time resolution. The TOF detector is capable of additional separation of ^{12}C and ^{13}C background ions.

Beam diagnostics is a weak point of the BINP AMS. There is only an off-axis ^{13}C Faraday cup, and beam optimization is provided by maximizing ^{13}C current and ^{14}C count. It is the ion source and beam diagnostics that is currently being developed in BINP AMS.

A comparison of the main design features of the two AMS facilities made it possible to reveal the importance of several features that significantly increase the performance of work on the MICADAS relative to the BINP AMS. These are a high degree of automation that greatly simplifies tuning of the facility; a negative ion source with high operation ^{12}C LE current that increases the statistical accuracy of measurements; a vacuum lock with separate pumping system and pneumatically driven vacuum gates that reduces the changing downtime of the samples. Thus, in order to achieve high performance of ^{14}C measurement together with high accuracy, any AMS facility must have all of the features listed above.

GIRI Test in AMS Golden Valley Laboratory

The AMS Golden Valley radiocarbon analysis laboratory participated in radiocarbon intercomparison for the first time. To check all possible toolkits during the Glasgow International Radiocarbon Intercomparison, we conducted three series of experiments: (1) AGE-3 + MICADAS-28, (2) ACS + MICADAS-28, and (3) AGE-3 +BINP AMS, with the maximum possible number of samples. Here the results on AMS-dating of the first and third series are presented. Sample preparation is described in detail in Parkhomchuk et al. (forthcoming) in this conference proceedings.

AMS-measurements for all graphite targets were made following our routine measurement sequence on MICADAS and BINP AMS. OX-I (SRM 4990B) was used as a modern standard material, and Polyethylene STD (BN 268530 Thermo Scientific) was used as a background reference material. The results from MICADAS-28 were analyzed using the BATS, the data reduction software, that is provided with MICADAS. Since this was the first time we went through the intercomparison and, in order to avoid accidental sample confusion, we prepared two or even more graphite probes from most samples if there was enough material. F^{14}C and

radiocarbon age measurements from both AMSs were compared with each other and with preliminary consensus GIRI-results (Scott et al. forthcoming), and the statistical significance was below 0.05 for samples O and Q measured on BINP AMS, with the other samples having no or minor differences according to the t-test results (see supplementary materials).

RESULTS AND DISCUSSION

Table 2 presents the results of GIRI samples graphitized by AGE-3 and then measured on MICADAS-28 and BINP AMS. $\delta^{13}C$ measured by MICADAS-28 for graphite targets was used to reduce the BATS data. BATS automatically calculates standard and blank corrected results for measured samples. The $\delta^{13}C$ data obtained on MICADAS-28 for graphites was used for calculating $F^{14}C$. Due to the lack of the possibility of manual input of fractionation value in BATS, $\delta^{13}C = -19.3‰$ for the standard OXI was used in BATS as nominal. $\delta^{13}C$ for all samples and $\delta^{15}N$ for the collagen was measured before graphitization by Delta-V-Advantage relative to the ANU sucrose and IVA Urea standards, respectively. $\delta^{13}C$ and $\delta^{15}N$ were normalized to VPDB scale and atmospheric nitrogen, respectively. $\delta^{13}C$ data from Delta-V-Advantage was used for $F^{14}C$ correction for all GIRI samples, measured by BINP AMS, OXI data was corrected to $\delta^{13}C = -19.3‰$. It can be seen that the average value for duplicated samples measured with BINP AMS is quite consistent with MICADAS and the preliminary results of GIRI (Scott et al. forthcoming). The errors of the results of the BINP AMS are larger compared with MICADAS due to the smaller statistics collected. On BINP AMS, we have systematic measurement errors, presumably related to the inaccuracy of normalization to the ^{13}C current due to the low beam stability. The latter is due to the inaccuracy of cathode positioning in the ion source and the drift of the X-Y stirrer high-voltage power supply. This phenomenon is better seen when measuring modern or labeled samples. For example, the standard deviations calculated for $F^{14}C$ measurements of ANU samples on the MICADAS and on the BINP AMS are 0.0037 and 0.0676, respectively (Figure 3).

Figure 3 presents the standards and blank results measured since 2021 on MICADAS-28 and BINP AMS, graphitized on AGE-3. Due to the commercial unavailability of the OXI standard, sucrose IAEA-C6 (ANU) is usually used as an internal standard for routine measurements on both MICADAS and BINP AMS, while OXI was used only for the GIRI test. The situation is similar with blank samples: we used local graphite MPG-6. It is fine-grained dense graphite made by cold pressing of graphite powder. It has higher physical and chemical parameters than those of other fine-grained analogues. After the GIRI test, the graphite blank was changed to polyethylene, which is closer to biomaterials analyzed for AMS by its chemical composition. Before launching the AGE-3 and MICADAS-28 at NSU, all the samples were graphitized by ACS and measured by BINP AMS. $F^{14}C$ for MPG-6 graphite as a blank graphitized during 2016–2021 is presented in Figure 4.

CONCLUSIONS

The AMS Golden Valley laboratory's participation in radiocarbon intercomparison for the first time is reported, with all possible toolkits checked during the Glasgow International Radiocarbon Intercomparison. Results of testing two types of accelerator mass-spectrometers have been presented. MICADAS-28 favorably differs from BINP AMS with better stability of blank and standard results and higher precision due to larger counting statistics and higher level of automation. The first Russian AMS built by BINP SB RAS in 2011 has demonstrated

Table 2 Results of GIRI samples graphitized by AGE-3 and then measured on MICADAS-28 and BINP AMS, together with the data on $\delta^{13}C$ measured by MICADAS-28 and Delta-V-Advantage. F = the measured fraction modern with fractionation correction applied to both the sample and standard and corrected for background. Uncertainties represent 1 sigma.

Name/ lab ID	Intersection (Scott et al. forthcoming)	Description	δ13C (‰)		F value This work		Radiocarbon age (BP) This work		Preliminary consensus GIRI[1] (Scott et al. forthcoming)
Set 1			Delta-V	MICADAS	MICADAS	BINP AMS	MICADAS	BINP AMS	
A GV-3799	TIRI A	Barley mash	−26.0	−24.4 −23.0	1.1644 ± 0.0042 1.1633 ± 0.0042	1.174 ± 0.007 1.193 ± 0.007	—	—	1.1643 ± 0.0075[5]
B GV-3800	VIRI U	Humic acid[2]	−29.7	−28.9 −29.9	0.2294 ± 0.0012 0.2291 ± 0.0012	0.221 ± 0.003 0.212 ± 0.003	11826 ± 41 11837 ± 41	12110 ± 115 12460 ± 120	11813 ± 110
C GV-3801		Barley mash	−28.0	−29.3	1.0075 ± 0.0041	1.075 ± 0.007 1.017 ± 0.007	—	—	1.0227 ± 0.0072[5]
D GV-3802		Humic acid[2]	−28.5	−26.7 −27.7	0.6226 ± 0.0025 0.6227 ± 0.0024	0.617 ± 0.005 0.588 ± 0.005	3807 ± 32 3805 ± 31	3883 ± 69 4269 ± 70	3826 ± 70.5
E GV-3803	SIRI F,G,H	Dendro-dated wood	−26.0	−23.7 −25.1	0.9569 ± 0.0035 0.9558 ± 0.0035	0.92 ± 0.006 0.99 ± 0.007	354 ± 30 364 ± 29	670 ± 54 56 ± 54	378 ± 48.56
F GV-3804		Barley mash	−26.6	−26.2 −27.0	1.0185 ± 0.0037 1.0162 ± 0.0037	0.994 ± 0.007 1.064 ± 0.007	—	—	1.0162 ± 0.0117[5]
G GV-3805	TIRI B FIRI D	Dendro-dated wood	−23.4	−22.0 −21.8 −18.7	0.5670 ± 0.0023 0.5710 ± 0.0023 0.7590 ± 0.0029	0.555 ± 0.005 0.583 ± 0.006	4558 ± 32 4501 ± 32 2210 ± 30	4726 ± 71 4340 ± 84	4523 ± 48.5
J GV-3808		Kauri wood	−21.7	−20.9 −20.3 −22.9	0.0085 ± 0.0006 0.0087 ± 0.0006 0.0084 ± 0.0006	0.0088 ± 0.0008 0.009 ± 0.0009	38265 ± 545 38109 ± 535 38364 ± 553	38070 ± 555 37630 ± 595	38571 ± 886
K(1)[3] GV-3809	TIRI L	Whalebone	−14.8	−15.1 −12.2	0.2029 ± 0.0011 0.2025 ± 0.0011	0.209 ± 0.004 0.222 ± 0.004	12814 ± 44 12827 ± 45	12560 ± 146 12100 ± 144	12780 ± 114
K(2)[4] GV-3809				−14.2 −15.6	0.2047 ± 0.0011 0.2019 ± 0.0011	0.205 ± 0.004 0.208 ± 0.004	12743 ± 44 12852 ± 44	12730 ± 142 12620 ± 140	
M GV-3811	VIRI O	Dendro-dated cellulose[2]	−25.5	−25.1 −24.1	0.9828 ± 0.0038 0.9813 ± 0.0038	0.986 ± 0.008 1.016 ± 0.008	140 ± 31 152 ± 31	110 ± 62 —	132 ± 32
N GV-3812		Kauri wood	−22.1	−23.6 −22.9	0.0018 ± 0.0006 0.0024 ± 0.0006	0.003 ± 0.0007 0.0009 ± 0.00006	>52000	>50000	0.002146 ± 0.00181[5]
Q GV-3813		Dendro-dated wood; single ring	−23.4	−25.6 −24.6	0.9601 ± 0.0038 0.9589 ± 0.0037	1.019 ± 0.008 1.012 ± 0.007	327 ± 31 337 ± 31	— —	336 ± 46
O GV-3814	FIRI E	Humic acid[2]	−29.9	−30.0 −29.7	0.2301 ± 0.0012 0.2312 ± 0.0012	0.204 ± 0.003 0.203 ± 0.003	11802 ± 41 11765 ± 41	12750 ± 120 12810 ± 119	11826 ± 153
P GV-3815	FIRI H	Dendro-dated wood	−24.4	−23.5 −24.7	0.7585 ± 0.0030 0.7582 ± 0.0030	0.762 ± 0.007 0.806 ± 0.007	2221 ± 32 2223 ± 32	2184 ± 69 1729 ± 67	2227 ± 62

[1]Taken as mean ± stdev.
[2]Pretreatment not required.
[3]$\delta^{15}N = 12.8‰$; C/N = 3.2.
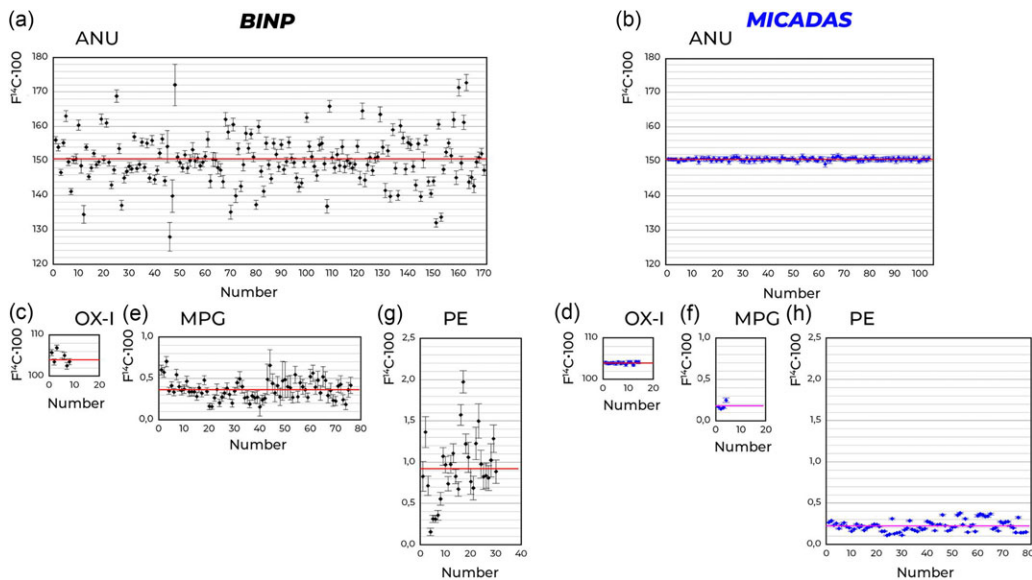[4]$\delta^{15}N = 12.7‰$; C/N = 3.2.
[5]Given as F.

Figure 3   F^{14}C·100 for standards and blanks, graphitized on AGE-3 and measured on BINP AMS (black) and MICADAS-28 (blue): (a) Sucrose IAEA-C6 (ANU) standards, measured on BINP AMS June 2021 to July 2022, (b) Sucrose IAEA-C6 (ANU) standards, measured on MICADAS-28 April 2021 to November 2022, (c) Oxalic acid (OX-I) standards, measured on BINP AMS April 2022 for GIRI test, (d) Oxalic acid (OX-I) standards, measured on MICADAS-28 March 2022 for GIRI test, (e) Blanks MPG-6 graphite, measured on BINP AMS June 2021 to November 2021, (f) Blanks MPG-6 graphite, measured on MICADAS-28 April 2021, (g) Blanks Polyethylene STD (BN 268530 Thermo Scientific), measured on BINP AMS February 2022 to July 2022, (h) Blanks Polyethylene STD (BN 268530 Thermo Scientific), measured on MICADAS-28 March 2022 to November 2022.
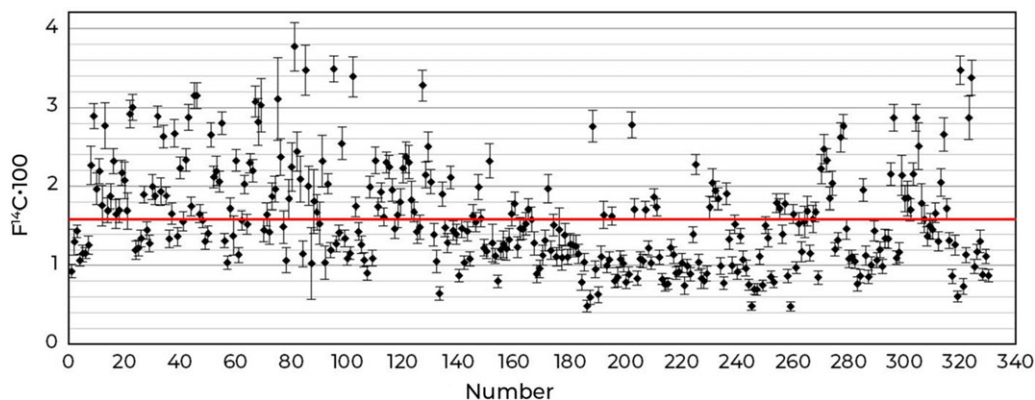

Figure 4   F^{14}C·100, measured on BINP AMS, for blank (MPG-6 graphite) graphitized on ACS 2016–2021.

the results comparable with ones of MICADAS-28 with enough degree of reproducibility. However, it inevitably requires further improvements in stability of power supply, ion source design, and AMS control system.

ACKNOWLEDGMENTS

SUPPLEMENTARY MATERIAL

To view supplementary material for this article, please visit https://doi.org/10.1017/RDC.2024.4

REFERENCES

Klyuev VF, Parkhomchuk VV, Rastigeev SA. 2009. A magnesium vapor charge-exchange target for an accelerator mass spectrometer. Instruments and Experimental Techniques. 52:245–248. https://doi.org/10.1134/S0020441209020225

Lysikov AI, Kalinkin PN, Sashkina KA, Okunev AG, Parkhomchuk EV, Rastigeev SA, Parkhomchuk VV, Kuleshov DV, Vorobyeva EE, Dralyuk RI. 2018. Novel simplified absorption-catalytic method of sample preparation for ams analysis designed at the Laboratory of Radiocarbon Methods of Analysis (LRMA) in Novosibirsk Akademgorodok. International Journal of Mass-Spectrometry. 433:11–18. https://doi.org/10.1016/j.ijms.2018.08.003

Molodin VI, Nenakhov DA, Mylnikova LN, Reinhold S, Parkhomchuk EV, Kalinkin PN, Parkhomchuk VV, Rastigeev SA. 2019. The Early Neolithic complex on the Tartas-1 site: results of the AMS radiocarbon dating. Archaeology, Ethnology & Anthropology of Eurasia. 47(1):15–22. https://doi.org/10.17746/1563-0110.2019.47.1.015-022

Nazarov EI, Kruzhalov AV, Vasyanovich ME, Ekidin AA, Kukarskikh VV, Parkhomchuk EV, Petrozhitsky AV, Parkhomchuk VV. 2022. ^{14}C in tree rings in the vicinity of the nuclear facility deployment areas. Izvestiya Wysshikh Uchebnykh Zawedeniy, Yadernaya Energetika 2022(1):107–117. https://doi.org/10.26583/npe.2022.1.09

Parkhomchuk EV, Gulevich DG, Taratayko AI, Baklanov AM, Selivanova AV, Trubitsyna TA, Voronova IV, Kalinkin PN, Okunev AG, Rastigeev SA, Reznikov VA, Semeykina VS, Sashkina KA, Parkhomchuk VV. 2016. Ultrasensitive detection of inhaled organic aerosol particles by accelerator mass spectrometry. Chemosphere 159:80–88. https://doi.org/10.1016/j.chemosphere.2016.05.078

Parkhomchuk EV, Petrozhitskiy AV, Ignatov MM, Kuleshov DV, Lysikov AI, Okunev AG, Babina KA, Parkhomchuk VV. Forthcoming. ^{14}C GIRI samples in AMS Golden Valley: graphite preparation using AGE-3 and absorption-catalytic setup. Radiocarbon.

Parkhomchuk VV, Rastigeev SA. 2009. Analysis of the ion background in an acceleration mass spectrometer of the Siberian Division of the Russian Academy of Sciences. Technical Physics 54:1529–1533. https://doi.org/10.1134/S1063784209100181

Parkhomchuk VV, Rastigeev SA. 2011. Accelerator mass spectrometer of the center for collective use of the Siberian Branch of the Russian Academy of Sciences. Journal of Surface Investigation 5 (6):1068–1072. https://doi.org/10.1134/S1027451011110140

Scott EM, Naysmith P, Dunbar E. Forthcoming. Preliminary results from Glasgow International Radiocarbon Intercomparison. Radiocarbon.

Shnaider SV, Zhilich SV, Zotkina LV, Boxleitner KA, Taylor WTT, Sayfullaev N, Koval VV, Baranova SV, Chernonosov AA, Kutnyakova LA, Tonasso-Calviere L, Orlando L, Spengler R. 2023. Occupation of highland Central Asia: new evidence from Kurteke rockshelter, Eastern Pamir. Archaeological Research in Asia 34:100443. https://doi.org/10.1016/j.ara.2023.100443

Synal H-A, Stocker M, Suter M. 2007. MICADAS: a new compact radiocarbon AMS system. Nuclear Instruments and Methods in Physics Research Section B: Beam Interactions with Materials and Atoms 259(1):7–13. https://doi.org/10.1016/j.nimb.2007.01.138

Wacker L, Nemec M, Bourquin J. 2010. A revolutionary graphitization system: Fully automated, compact and simple. Nuclear Instruments and Methods in Physics Research Section B: Beam Interactions with Materials and Atoms 268:931–934. https://doi.org/10.1016/j.nimb.2009.10.067